THE JOURNAL OF PHYSICAL CHEMISTRY C

Article

pubs.acs.org/JPCC

Exact Analysis of Nanoantenna Enhanced Fluorescence Correlation Spectroscopy at a Mie Sphere

Lutz Langguth, Clara I. Osorio, and A. Femius Koenderink*

Center for Nanophotonics, FOM Institute AMOLF, Science Park 104, 1098 XG Amsterdam, The Netherlands

ABSTRACT: In fluorescence correlation spectroscopy (FCS), one measures and correlates the fluctuations that occur as fluorophores diffuse into and out of the detection volume of a microscope. The resulting correlations are used to determine concentrations and diffusion rates of fluorescent species in liquid environments. The sensitivity of this technique is limited by the field intensity and the dimensions of the detection volume, both of which can be modified by nanostructures through geometric and plasmonic effects. In this paper we aim to establish how far noble metal Mie spheres, acting as plasmon antennas, can boost FCS. To that end, we model a realistic scenario that takes into account the exact solutions of the field near a plasmon antenna, the modified diffusion owing to the antenna excluding volume, as well as quantum efficiency and local density of states (LDOS) effects.

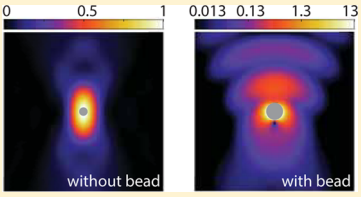

INTRODUCTION

Fluorescence correlation spectroscopy (FCS) is a noninvasive optical technique used to measure concentrations and diffusion constants of fluorescent samples highly diluted in liquid environments.[1,2] In standard FCS, a confocal microscope defines diffraction limited excitation and detection volumes inside the solution in which the fluorescent solute of interest is diffusing.[2,3] As fluorophores diffuse into and out of focus, the detected intensity fluctuates. The second order temporal correlation function of the detected random stream of photons shows an excess correlation with a roll-off time set by the diffusion constant and a magnitude (or contrast) that is inversely proportional to the concentration.[3,4] Since the correlation can be traced to the diffusion of individual solutes, a strong contrast requires concentrations comparable to one per detection volume. Performing FCS at concentrations above the nanomolar range requires detection volumes significantly smaller than the diffraction limited focus of the microscope, which is challenging.

Nanohole antennas in metal films, and other plasmonic structures, have proven to be a useful tool for FCS.[5−10] These nanostructured metals have strong optical resonances, which are mediated by the resonant response of free electrons near the plasma frequency.[11] Plasmonic structures offer two different mechanisms to improve standard FCS.[8] On the one hand, reduction of the detection volume (up to $\lambda/20$) and geometric confinement raise the concentration range in which FCS is applicable, as first demonstrated by Levene et al.[5] On the other hand, the enhancement of electromagnetic fields in small volumes[8,9,12−16] boosts absolute fluorescent count rate, increasing brightness per molecule up to 1000-fold.[15−18] In addition to the striking improvements on FCS shown using holes in thick metal films, several authors have proposed that similar enhancements can be obtained with single metal particles, even though these structures do not provide geometrical confinement.[7,17,19−21] Detection volume reductions (with respect to a plasmon-free case) ranging from factors of 2 to as much as 10^4 have been reported, when using simple metal nanospheres and nanorods as antennas.[7,19,20]

Given this huge disparity between claimed plasmon-enhancements in FCS, an important question is how to interpret increased FCS correlation contrast and reduced roll-off times in terms of electromagnetic field enhancement and confinement. To date, the main approach is to approximate the electromagnetic focus as a Gaussian function, ignoring that diffusion near a plasmon particle is hindered as compared to free diffusion.[2,3] In this work, we assess the actual FCS enhancements obtainable with a metallic Mie particle as plasmon antenna. We rigorously account for the effect of the antenna (and its geometric exclusion region) on the pump field, for the modified diffusion behavior, as well as for local density of states and quenching effects, which are expected to occur where the field enhancement is highest.[22] To this end, we calculated semianalytically the field intensity distribution for a metal Mie particle in a tight focus, as well as the diffusion kernel in the presence of a spherical nanoparticle. These factors are combined to predict optical excitation and detection efficiency functions and correlation time traces.

This paper is organized as follows. After introducing the basic concepts of confocal FCS, we rigorously describe the effects of a plasmonic particle on the excitation function, on the molecular detection efficiency, and on the geometry of diffusion. In each of these three cases, we consider how the effect of the particle translates to the FCS traces. In the case of the molecular detection efficiency, we take into account additional effects due to spontaneous emission rate enhancements and quenching. On the other hand, when considering the geometrical effects, we demonstrate that the resulting modification of the diffusion kernel has a moderate effect on the FCS traces. We finish the paper by comparing the

Received: March 1, 2016
Revised: June 2, 2016
Published: June 7, 2016

DOI: 10.1021/acs.jpcc.6b02186
J. Phys. Chem. C 2016, 120, 13684−13692

rigorously calculated FCS traces to common Gaussian hotspot approximations.

RESULTS AND DISCUSSION

Confocal FCS. To review the basic concepts of confocal FCS, consider a sample with a fluctuating concentration of fluorophores (with a mean concentration C). As the fluorescence fluctuates, the time-dependent detected intensity $I(t)$ has an autocorrelation defined as[1−4,23]

$$G(\tau) = \frac{\langle I(t)I(t+\tau)\rangle}{\langle I(t)\rangle^2}$$

and given by

$$G(\tau) = \frac{1}{C}\frac{\int \mathrm{MDF}(\mathbf{r})K(\mathbf{r},\mathbf{r}',\tau)\mathrm{MDF}(\mathbf{r}')\,\mathrm{d}^3\mathbf{r}\,\mathrm{d}^3\mathbf{r}'}{\int \mathrm{MDF}(\mathbf{r})\,\mathrm{d}^3\mathbf{r}\int \mathrm{MDF}(\mathbf{r}')\,\mathrm{d}^3\mathbf{r}'} \quad (1)$$

Here $K(\mathbf{r},\mathbf{r}',\tau)$, which is the kernel of the diffusion equation, represents the probability that an object that started diffusing from $\mathbf{r}'$ has reached $\mathbf{r}$ a time τ later. The combined "molecular detection function" MDF specifies the spatial selectivity of the optical excitation and detection process.[3] The MDF can be factorized as a product of two contributions. First, the "excitation efficiency function" EEF quantifies the likelihood of a molecule at a position $\mathbf{r}$ to be excited, given the intensity profile of the incident focused beam. Second, the "collection efficiency function" CEF gives the probability with which an excited molecule at $\mathbf{r}$ actually yields a photon detection event, thereby quantifying the spatial selectivity of the detection scheme. It is common to define MDF as a normalized probability distribution function, putting aggregate effects such as the detector quantum efficiency, emitter cross section, and so forth in a prefactor that is not relevant for the amplitude of the normalized autocorrelation $G(\tau)$.

In confocal FCS, often a single pinhole defines the excitation and the collection efficiencies (EEF and CEF), which are therefore considered as identical Gaussians of diffraction limited width. In that case, the detection function MDF $\propto \exp(-2r^2/\sigma^2)\exp(-2z^2/(s\sigma)^2)$, where r represents the transverse coordinate, z the axial direction, σ the focal width, and $s \approx 2$ the ratio of the axial and radial focal dimension. For free diffusion, where the diffusion kernel is also Gaussian, this assumption leads to the standard expression[2,10]

$$G(\tau) = \frac{\langle N\rangle}{(1+\tau/\tau_\mathrm{D})\sqrt{1+\tau/(s^2\tau_\mathrm{D})}} \quad (2)$$

The correlation at zero-delay $G(0)$ is identified as the mean number of molecules in the effective focal volume $V_\mathrm{eff} = \pi^{3/2}s\sigma^3$, and $\tau_\mathrm{D} = \sigma^2/(4D)$ is a measure for the time required to diffuse across the focus. Experimentally, one retrieves $G(0)$ from the zero-time contrast of a measured correlation curve, and τ_D from the roll-off time of the curve, which is the time τ' for which $G(\tau') = G(0)/2$.

In this work, we consider the effects of modifying confocal FCS by placing a Mie particle at the center of the focus. In the following sections we show how the sphere modifies the focus itself, the excitation and collection efficiencies (EEF, CEF), as well as the diffusion kernel $K(\mathbf{r},\mathbf{r}',\tau)$.

Plasmonic Modification of the Excitation Efficiency Function. Let us start by considering how the plasmonic particle modifies the focus in which it is placed. To model a concrete experiment, we consider a gold nanosphere of radius a = 50 nm as Mie particle and we assume the sphere to be immersed in water and use the diffusion constant of rhodamine 6G dye in water ($D = 4 \times 10^{-10}$ m^2/s). We use the optical constants from Johnson and Christy[24] and assume as wavelength 567 nm, the Ar/Kr laser line closest to the plasmon resonance.

The near field of a spherical scatterer excited by a plane wave polarized along x and propagating along the z-axis is exactly given by

$$\mathbf{E}_\mathrm{Mie} = \mathbf{E}_x e^{ikz} + \sum_{n=1}^{\infty}\sum_{m=-n}^{n}\left[a_n\mathbf{N}_{nm}(r,\theta,\phi) + b_n\mathbf{M}_{nm}(r,\theta,\phi)\right] \quad (3)$$

where a_n and b_n are the well-known Mie coefficients[25] and $\mathbf{N}_{nm}(r,\theta,\phi)$, $\mathbf{M}_{nm}(r,\theta,\phi)$ are the vector spherical harmonic basis functions, which are described by C. T. Tai[26] and in other textbooks. Given that a high numerical aperture (NA) focus can be represented as a sum of plane waves, we construct the near field of the Au particle in a focused field as a linear superposition of Mie solutions, using the fact that a high NA focus reads[27]

$$\mathbf{E}_\mathrm{f}(x,y,z) \propto \iint_{|\mathbf{k}_\parallel|\cdot n/|\mathbf{k}|<\mathrm{NA}} \mathrm{d}\mathbf{k}_\parallel \frac{E(k_x,k_y)}{|\mathbf{k}_\parallel|^2\sqrt{|\mathbf{k}|k_z}} \times \exp[i\mathbf{k}_\parallel\cdot(x,y) + ik_z z]\begin{pmatrix} k_y^2 + k_x^2 k_z/|\mathbf{k}| \\ k_x k_y(k_z/|\mathbf{k}| - 1) \\ -(k_x^2 + k_y^2)k_x/|\mathbf{k}| \end{pmatrix} \quad (4)$$

where we take $E(k_x,k_y)$ constant over the back aperture of the focusing lens, and we defined $|\mathbf{k}| = (\omega/c)n$, $\mathbf{k}_\parallel = (k_x,k_y)$, and $k_z = [|\mathbf{k}|^2 - |\mathbf{k}_\parallel|^2]^{1/2}$. We use a numerical evaluation of this integral as input for the FCS correlation integrals that are shown later. We refer to the Methods section for numerical implementation details regarding the FCS correlation integrals.

Figure 1 compares the electromagnetic field obtained by coherent superposition of plane waves without and with the plasmonic enhancement of the sphere while considering its exclusion volume. Without plasmonic enhancement, as in Figure 1a, the sum results in a diffraction-limited focus with a full width at half-maximum (fwhm) of 260 and 495 nm in the transverse and axial direction, respectively. The exact geometry of the weak fringes around the focus depends on the chosen apodization of the input beam which, in an experiment, will be further modified by aberrations (refs 28 and 29 present a quantitative study of these effects). In the presence of the plasmonic nanoparticle (Figure 1b), the field distribution $|E|^2$ shows two lobes on either side of the particle surface (along the polarization direction) with a moderate enhancement of $|E|^2 \sim 13$ compared to the incident field, due to the dipolar plasmon resonance. Additionally, a standing wave pattern evident on the incident side $z > 0$ is formed by the sum of the incident wave and the strong back-scattered field. This kind of pattern is expected for large Au nanoparticles on resonance, which have high scattering efficiencies and cross sections close to the diffraction limit.

Having calculated the effect of the sphere on the pump field distribution, we consider the effect of this modified field on the expected FCS curves. To that end, we evaluate eq 1 taking the calculated pump field $|E(r)|^2$ as the excitation efficiency function EEF, setting the collection efficiency function CEF

DOI: 10.1021/acs.jpcc.6b02186
J. Phys. Chem. C 2016, 120, 13684−13692

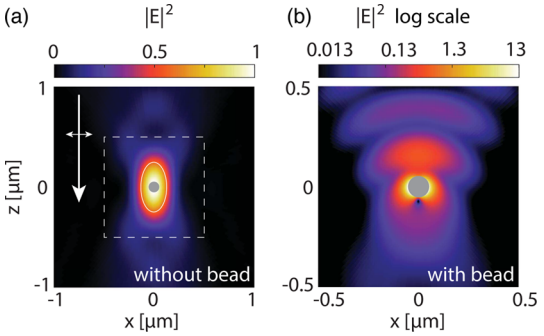

Figure 1. Focal field intensity calculated using plane wave reconstruction assuming λ = 568 nm, n = 1.33, and an input NA = 0.95, n = 1.26. The cut shown is in the xz plane, with x-polarized illumination incident from above. Panel a shows the field considering the exclusion volume but not the particle's plasmonic enhancement. The ellipse indicates the 50% contour of the field (width and length of 260 and 495 nm, respectively). In panel b, the calculated total field in presence of the 100 nm Au Mie sphere shows a 13-fold field enhancement at the particle edge compared to the bare focus. The field rapidly decays within 10 nm when moving away from the particle. For this reason, the area shown in panel b is smaller than in panel a and the color scale used is logarithmic. The dashed square in panel a indicates the region for which the field plot in panel b is generated.

to a constant, and using a free-space Gaussian diffusion kernel. This model describes an experimental setup without confocal pinhole in the detection optics.

First, consider the effect of approximating the excitation function EEF to a Gaussian, as commonly done in FCS. Without plasmonic enhancement, the blue line in Figure 2 is

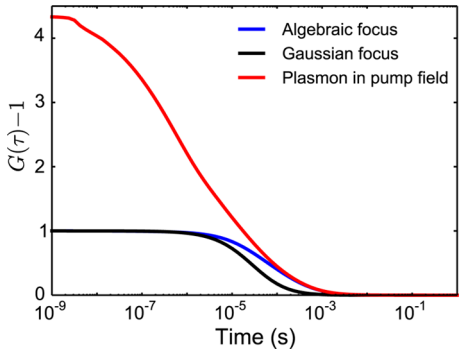

Figure 2. FCS traces calculated presupposing that only the pump focus is confined, and there is no confocal detection pinhole. Blue line: Calculated FCS trace expected for the microscope focus synthesized by linear superposition of plane waves. Black solid line: Gaussian focus FCS curve with no adjustable parameters taking the dimensions from the $1/e^2$ contour of the focal intensity distribution. While we plot the analytic expression, we also calculated the result by numerical integration using the same routines as for the full result. The analytic and numerical results are equal at all times to within a few percent. Red line: same but now including the field intensity enhancement at the plasmon particle in the EEF. Note that to obtain this result, we use the free diffusion kernel.

the expected FCS curve when using the field in Figure 1a as EEF. The black line shows the FCS curve expected when approximating EEF to a Gaussian setting s = 2 and σ = 223 nm (taken from the $1/e^2$ contour of the calculated focal field and without using other adjustable parameters).

The roll-off time of the FCS trace (defined as the time τ for which $G(\tau) - 1 = {}^1/_2$) changes from τ = 54 μs, when considering the calculated focal field, to τ = 23.8 μs for its Gaussian approximation. This discrepancy is not due to the fact that the calculation excludes the volume of the sphere (also in the nonplasmonic case), as verified below, and by independent calculations (not shown). Instead, this discrepancy indicates that the calculated focal field has a much larger effective focus size than the Gaussian approximation, as suggested by the results of ref 28, which analyzes the dependence of FCS traces on focus nonidealities and pinhole choice. In fact, the focus created by linear superposition of plane waves has a much less pronounced field decay away from the focus in both the transverse and axial direction than a true 3D Gaussian. Figure 2 shows a normalized FCS curve for the nonapproximated focus (i.e., concentration tuned to obtain contrast 1 at zero time), and the calculation also provides the effective volume of the focus. Expressed in linear dimensions the focus has $[V_{\mathrm{eff}}/\pi^{3/2}]^{1/3}$ = 425 nm.

Next, consider the plasmonic enhancement. The red line in Figure 2 is the FCS curve expected when *including* the plasmonic enhancement in the excitation efficiency, keeping the collection efficiency function CEF as a constant. The plasmon-enhanced pump field gives a contrast enhancement of ~4.4 compared to the case without any enhanced field (blue line). The long-time tail of the plasmon FCS curve (red line) exactly overlaps that for the focus in absence of any particle (blue line), indicating a large contribution of the background focus to the excitation volume. Furthermore, in contrast to predictions of simple Gaussian models, the FCS curve does not flatten at microsecond timescales, with flattening only noticeable at very short times, in the 5−10 ns range. The relevance of such short time scales in the FCS curve indicates strong field changes on distances of a few nanometers from the particle ($\sim r^2/D \sim$ 5 ns for a length scale $r \sim$ 1.5 nm). Regarding the 4-fold contrast enhancement at zero delay, intuitively it seems disappointingly small, since the actual hotspot volume and focal volume stand in a 1:60 ratio. However, as already noted by Langguth et al.,[10] the correlation enhancement is suppressed because at moderate field enhancements, the background focus contributes substantially to the signal. Figure 2 also shows that the roll-off time (50% point) of the simulated FCS trace ($\tau \approx$ 2.1 μs) is a factor 25 shorter than that for the bare focus. The apparent reduction in volume estimated from the roll-off time is about a factor 130 larger than that estimated from the 4-fold change in contrast. The roll-off time and contrast are very differently affected by the mixing of hotspot contributions and focus contributions to the FCS signal, as shown in ref 10 for a simple model of a Gaussian-shaped hotspot superimposed on a Gaussian beam. In addition, the standing wave lobe in front of the particle also contributes to the FCS signal.

To conclude, nanoparticle FCS traces are substantially different from what is expected on the basis of hotspot field enhancement and extent in simple Gaussian models. While the apparent discrepancy between contrast enhancement and roll-off time reduction is qualitatively well captured by a multi-Gaussian approximation for the *sum* of hotspot and focus, an additional complicating factor is that the temporal decay of the correlation has many short time scales, indicative of large field gradients. These would be difficult to resolve in actual measurements, as one approaches fluorescence and triplet rates.

Role of LDOS and Quantum Efficiency in the Collection Efficiency. In the previous section, we only

DOI: 10.1021/acs.jpcc.6b02186
J. Phys. Chem. C 2016, 120, 13684−13692

considered the contribution of the pump field to the FCS enhancement by taking into account structure in the excitation (EEF) but no spatial selectivity in the collection efficiency (CEF). In actual FCS measurements, however, the spatial selection of the confocal detection pinholes and the brightness enhancements induced by the plasmon particle result in a position dependence for the photon collection probability (CEF(**r**)). By use of reciprocity,[30] the detection probability enhancement can be related to the calculated pump focus distribution in a true confocal scheme, provided that the illumination and detection use the same confocal pinhole (and assuming a negligible effect from the Stokes shift between emission and absorption). Within these assumptions, the reciprocity theorem asserts that the radiation enhancement from a classical electrodynamic point dipole source of given current strength into any particular mode can be calculated by recording the local field enhancement at the dipole's location when the system is irradiated from that particular mode.[30,31] A molecule is, however, not a fixed current source but rather emits at most one photon per excitation cycle.[30,32,33] For a unit-quantum efficiency molecule (in the absence of any intrinsic or nanostructure induced quenching), reciprocity hence states that collection efficiency function CEF reads[23]

$$\mathrm{CEF}(\mathbf{r}) = \frac{|\mathbf{E}_{\mathrm{NP+focus}}(\mathbf{r})|^2}{\mathrm{LDOS}(\mathbf{r})} = \frac{\mathrm{EEF}(\mathbf{r})}{\mathrm{LDOS}(\mathbf{r})} \tag{5}$$

where the local density of optical states LDOS quantifies the power radiated by a constant current source in classical electrodynamics, and in optics it describes the enhancement of spontaneous emission decay rates. More strictly stated, in terms of the Green's function $\mathbf{G}(\mathbf{r},\mathbf{r})$, LDOS(**r**) denotes the quantity Tr(Im $\mathbf{G}(\mathbf{r},\mathbf{r})$) normalized to Tr(Im $\mathbf{G}$) of vacuum and averaged over dipole orientation.

For a real molecule, with an arbitrary intrinsic quantum efficiency ϕ_0, plasmon structures can accelerate radiative decay as well as induce quenching,[6,22,32] inducing a spatial dependence on the quantum efficiency. These effects lead to a collection efficiency function CEF given by

$$\mathrm{CEF}(\mathbf{r}) \propto \frac{|\mathbf{E}_{\mathrm{NP+focus}}(\mathbf{r})|^2}{\mathrm{LDOS}(\mathbf{r})}\phi(\mathbf{r}) \tag{6}$$

where the space-dependent quantum efficiency $\phi(\mathbf{r})$ can be written in terms of the decay rates. Denoting $\gamma_{\mathrm{tot}}(\mathbf{r})$ the total decay rate of the fluorophore (in absence of any plasmonic structure), the associated radiative and nonradiative rates are $\gamma_{\mathrm{r}}(\mathbf{r}) = \phi(\mathbf{r})\gamma_{\mathrm{tot}}(\mathbf{r})$ and $\gamma_{\mathrm{nr}}(\mathbf{r}) = (1 - \phi(\mathbf{r}))\gamma_{\mathrm{tot}}(\mathbf{r})$, while the total decay rate in presence of the plasmonic structure is

$$\gamma_{\mathrm{tot}}(\mathbf{r}) = \gamma_{\mathrm{nr}} + \gamma_{\mathrm{r}}\mathrm{LDOS}(\mathbf{r}) \tag{7}$$

and the radiative part of this enhanced rate is

$$\gamma_{\mathrm{r}}(\mathbf{r}) = \gamma_{\mathrm{r}}\mathrm{LRDOS}(\mathbf{r}) \tag{8}$$

Where the quantities γ_{nr} and γ_{r} without position dependence are the intrinsic nonradiative and radiative decay rate of the molecule, in absence of any plasmonic structure. In this last expression, we introduced LRDOS(**r**) as the radiative part of the local density of states, as defined by Mertens et al.[22] Consequently, the quantum efficiency in the presence of the plasmonic structure reads

$$\phi(\mathbf{r}) = \frac{\gamma_{\mathrm{r}}(\mathbf{r})}{\gamma_{\mathrm{tot}}(\mathbf{r})} = \frac{\phi_0\mathrm{LRDOS}(\mathbf{r})}{1 + \phi_0(\mathrm{LDOS}(\mathbf{r}) - 1)} \tag{9}$$

This equation summarizes two well-known facts: (1) at intrinsic quantum efficiency $\phi_0 = 1$, the quantum efficiency of the coupled system reads LRDOS/LDOS < 1, which implies no efficiency enhancement and, even worse, a significant quenching of efficient emitters by metal surfaces; (2) the quantum efficiency may be significantly enhanced at very low intrinsic quantum efficiency ($\phi_0 \ll 1$). Figure 3 shows the orientation-averaged LDOS and LRDOS for the Au sphere considered in this work, which was calculated using the analytical expressions from Mertens et al.[22] At the sphere surface, there is a finite LRDOS enhancement of nearly 15 while the LDOS diverges. Therefore, the effective quantum efficiency for the emission of any emitter reaches zero.

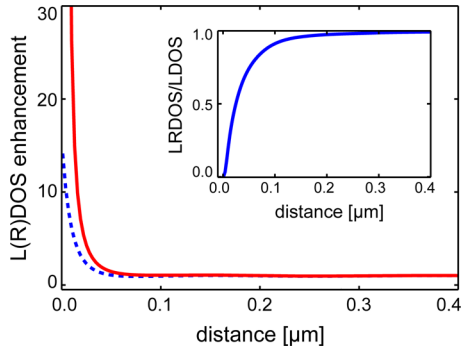

Figure 3. Local density of states (LDOS, red solid line) and radiative part of the local density of states (LRDOS, blue dashed line), both normalized to the host LDOS, as function of distance to the Au sphere. The inset shows the ratio of the two, which is equivalent to the quantum efficiency of emission assuming one brings a unit quantum efficiency emitter in proximity of the sphere.

We note that besides this electromagnetic quenching, there can also be quenching effects when molecular wave functions reach the metal, e.g., quenching due to direct electron transfer or due to chemical changes. As these would require a microscopic theory, these are not included here. In any case for FCS these changes would hardly matter, because they only occur at very short distance ranges (<1 nm) where anyway the quantum efficiency is quenched electromagnetically.

Molecular Detection Function in the Presence of a Mie Sphere. In the remainder of this paper, we consider the molecular detection function MDF = EEF × CEF and the FCS traces for two typical limits: a low quantum efficiency emitter ($\phi_0 = 0.01$) and a high quantum efficiency emitter ($\phi_0 = 1$). Figure 4 shows *xz* cuts of the apparent collection efficiency CEF (panels a and b) and MDF (panels c and d). Each panel is normalized to the peak value for the same molecule in the center of the focus and in the absence of any plasmon particle. When using a very poor emitter ($\phi_0 = 0.01$), the LRDOS enhancement of the particle increases the probability of emission of an excited dye approximately 5-fold (Figure 4a). The maximum enhancement occurs at a distance of about 10 nm away from the metal surface. At closer distances quenching dominates, and consequently, right at the particle surface the CEF (as well as the total MDF in Figure 4c) vanishes. The background focus contributes appreciably to the FCS signal because of its large volume, but it hardly appears in the figure because of the linear color scale used. When using a unit

DOI: 10.1021/acs.jpcc.6b02186
J. Phys. Chem. C 2016, 120, 13684−13692

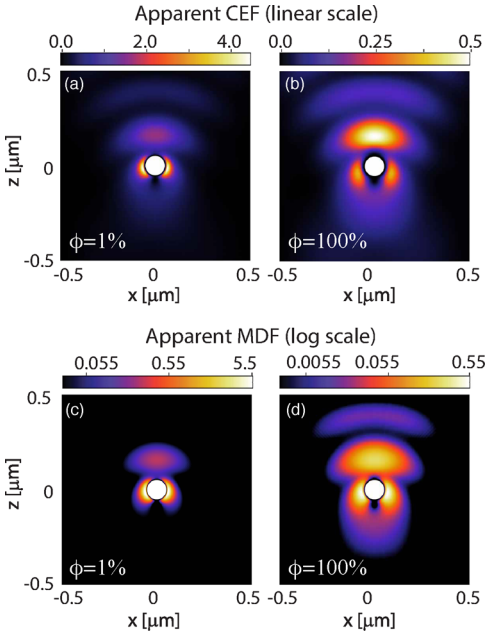

Figure 4. Collection efficiency function (CEF) for a 1% (a) and a 100% emitter (b) normalized to the CEF for a fluorophore at the focus in absence of any plasmon particle. A low efficiency emitter may experience an enhanced photon extraction yield, while the CEF of a high efficiency emitter is only adversely affected by the plasmon structure. The combined molecular detection function (MDF), a product of the CEF and the pump field enhancement EEF, is shown again for the case of a 1% (c) and a 100% emitter (d). Note that the MDF has sharper and more localized features, especially in the case of a low efficiency emitter, and therefore the top panels use a linear color scale while the lower panels use a logarithmic color scale (going down to 0.5% of the MDF maximum).

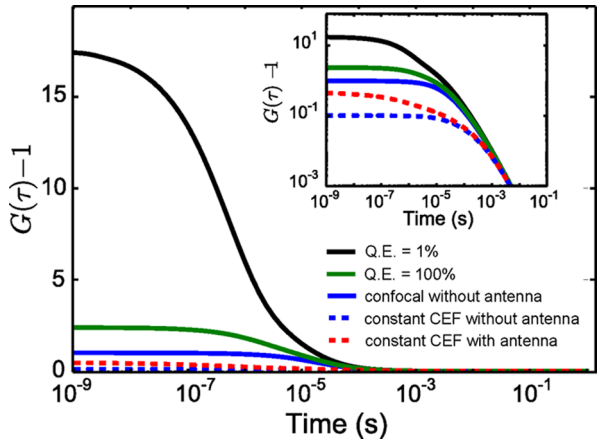

Figure 5. In black and green, FCS traces obtained when taking into account both pump field intensity enhancement in the EEF and the change in collection efficiency (CEF) after excitation. For reference, the solid blue curve shows a confocal but antenna-free trace. Dashed lines show traces obtained with a constant collection efficiency (CEF) and an excitation efficiency function (EEF) with (red) and without (blue) antenna. All curves assume the same molecular concentration (chosen to obtain unit contrast for the confocal pinhole case). For a high efficiency molecule (100% intrinsic quantum efficiency, green curve) the FCS contrast is 2.5-fold enhanced compared to that obtained when accounting only for pump field enhancement. For a low efficiency molecule (1% intrinsic efficiency, black curve), the contrast is much more strongly enhanced (17-fold). The inset shows the same curves on a log−log scale. All curves assume a free diffusion kernel.

quantum efficiency fluorophore, coupling to the particle reduces the quantum efficiency and the CEF is nowhere enhanced compared to a bare focus (Figure 4b). In the case that the field enhancement is due to a single and strong photonic resonance, no plasmon structure is likely to give any net photon extraction advantage for efficient emitters, as LDOS $\propto |E_{NP+focus}|^2$, leading to a cancellation of terms in eq 6. Rather than being set by the two typical dipolar lobes of the plasmon resonance, the CEF (panel b) is dominated by the first maximum of the reflected standing wave. Using the molecular detection function, we can now construct the full molecular detection and excitation efficiency function MDF, Figure 4c and Figure 4d. In front of the particle, the first maximum of the reflected standing wave contributes strongly to the MDF. Confinement of the MDF decreases as the quantum efficiency increases because the drastic reduction of quantum efficiency near the particle counters the field enhancement.

Figure 5 compares FCS curves obtained taking into account both pump field intensity enhancement in the EEF and the change in collection efficiency function CEF after excitation (green and black curves in the inset show the same curves on a log−log scale). All cases are normalized to a concentration with unity zero-time contrast of the background focus assuming a confocal pinhole (blue curve). This reference is different from that considered in Figure 2 because in that case no detection pinhole was assumed. The FCS trace for the full focus (blue solid curve) is almost identical to its Gaussian approximation (with $s = 2$ and $\sigma = (223\ \text{nm})/\sqrt{2}$ both directly taken from the $1/e^2$ level of the calculated focus) and shows an FCS contrast that is 9.8 times that of the no-pinhole case (blue dashed curve). The excellent correspondence further indicates that exclusion of volume by the particle does not appreciably change the FCS curve. This much larger contrast and the fact that the no-pinhole case is poorly fitted by a Gaussian model, while the pinhole-case is, underline the large relevance of a good confocal microscope geometry in standard FCS.

Returning to the plasmonic scenario, we note that the long time tails of all FCS curves are identical. The FCS signature of diffusion in the background focus explains that all curves overlap on time scales of 1 ms and longer. At shorter times, FCS contrast is enhanced when considering the plasmonic effects in the MDF, in the cases of low (black curve) and high (green curve) quantum efficiencies. Comparing to the plasmon free case (blue curve), there is a factor 2 enhancement in the contrast with 100% quantum efficiency and a factor 14 with 1% quantum efficiency fluorophores. For the 1% quantum efficiency case, there is a 140 times enhancement when compared to a reference measurement that does not use a confocal pinhole (blue dashed curve), which is the "worst possible" plasmon-antenna-free measurement. Regarding the flattening of the curves at short times, the QE = 1% curve already shows noticeable roll-off at 5 ns, indicating steep gradients in the MDF. In contrast, the QE = 100% curve only shows signs of roll-off at 50−100 ns, since the plasmon near field does not strongly contribute.

These examples show that a local increase of quantum efficiency strongly confines the molecular detection function to a thin shell around the metal particle, making possible significant FCS contrast enhancements. However, the maximum enhancement predicted by our full calculations is significantly lower than previous experimental results. Consider

DOI: 10.1021/acs.jpcc.6b02186
J. Phys. Chem. C 2016, 120, 13684−13692

for instance the 10 000-fold enhancement of FCS contrast reported in ref 7 for a fixed Mie sphere immobilized on a glass substrate. The presence of the substrate and particle shape variations could provide modest enhancements over the Mie sphere, but a factor 1000 difference is unexpected. Rather than being due to plasmonic effects, this unexpected large enhancement could also be due to physicochemical effects hindering diffusion such as adhesion, which can result in bright bursts yielding high FCS contrast. According to our calculations, with efficient dyes (Wang et al.[19] using Cy5) only very moderate enhancements are possible, while at best 2 orders of magnitude can be gained when using inefficient dyes.[16,20] The general behavior as a function of quantum efficiency can be quantified by casting the zero-delay time FCS contrast into an effective detection volume. Figure 6 shows the effective detection volume V_{eff} versus quantum efficiency, parametrized by the effective hotspot width

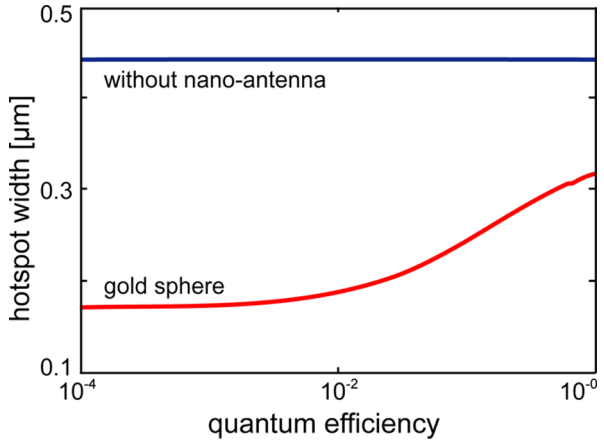

Figure 6. In traditional confocal FCS the effective detection volume, here parametrized using the hotspot width σ, is independenet of the quantum efficiency of the fluorescent species (blue), which is not the case when considering a nanoantenna in the focus (red).

$$\sigma = \frac{1}{\pi^{1/2}}(V_{\mathrm{eff}})^{1/3} = \frac{1}{\pi^{1/2}}\left(\frac{(\int \mathrm{MDF}(r)\ \mathrm{d}r)^2}{\int \mathrm{MDF}(r)^2\ \mathrm{d}r}\right)^{1/3}$$

For the background focus, the effective detection volume has width σ = 440 nm. In the presence of the gold sphere the volume of the hotspot is just 2.5 times smaller for efficient dyes (σ = 325 nm), while for quantum efficiencies below about 1% it plateaus at about 17.5 times volume reduction (σ = 170 nm).

Modified Diffusion Kernel near a Nanoparticle. So far we have accounted for electrodynamic effects on the excitation and collection efficiency of fluorophores while assuming that diffusion is unhindered by the presence of the sphere. In this section we validate this common assumption by comparing free diffusion results to calculations that take into account that the plasmon particle is impenetrable. The sphere might also modify diffusion because fluorophores tend to stick to antennas, which may cause measurement artifacts such as large run-to-run variations in FCS contrast. Since this type of artifact is easily avoided by use of surfactants, we disregard it in our analysis and focus on the excluded-volume effect only. Assuming fluorophores diffusing with diffusion constant D and an impenetrable, nonsticking sphere, the solution to the diffusion equation at a point $\mathbf{r} = (r,\theta,\phi)$ at time t for a δ-source located at $\mathbf{r}' = (r',\theta',\phi')$ and t' reads[23,34]

$$K_{\mathrm{a}}(r, r', \tau = t - t') = \frac{2}{\pi}\sum_{n=0}^{\infty}\sum_{m=-n}^{n} \int_0^{\infty} \mathrm{d}k\ k^2\ \exp[-Dk^2\tau]\psi_{n,m,k}(r,\theta,\phi)\psi^*_{n,m,k}(r',\theta',\phi') \tag{10}$$

where the basis functions

$$\psi_{n,m,k}(r,\theta,\phi) = Y_{nm}(\theta,\phi)\frac{y_n(ka)j_n(kr) - j_n(ka)y_n(kr)}{\sqrt{y_n'^2(ka) + j_n'^2(ka)}} \tag{11}$$

are given in terms of spherical harmonics $Y_{nm}(\theta,\phi)$, and $j_n(x)$ and $y_n(x)$ are respectively spherical Bessel functions of the first and second kind. As the sphere is impenetrable, this expression only holds for source and detection points outside the sphere. For small $\tau = t - t'$, the solution is close to a δ-singularity and the integral separates into two parts

$$K_{\mathrm{a}} = K_0 + [K_{\mathrm{a}} - K_0]$$

where the (analytically known) Gaussian diffusion kernel for free space $K_0(r,r',\tau)$ contains the singularity at zero time, while $K_{\mathrm{a}} - K_0$ is a smooth function, which we calculate using rapidly convergent numerical integration. Notice that this result will differ for NSOM tips or other cylindrical structures, as shown in previous works that considered the modified diffusion kernel and MDF for this kind of structures.[35−37]

Figure 7 shows the comparison between free diffusion and diffusion in presence of a sphere. Figure 7a considers the case in which the MDF is set by the pump field enhancement only, while Figure 7b shows the result accounting also for the CEF assuming fluorophore quantum efficiency 1%. Neglecting that the particle modifies diffusion has a considerable effect in the hypothetical case that only pump field modification matters for FCS, for which case Figure 7a shows a deviation up to 20%. Since the modification of the diffusion kernel is mainly localized right at the particle, the agreement is much better when considering the MDF instead of the EEF only, as done to calculate Figure 2. Indeed, since the effect of quenching suppresses contributions to the MDF right from the region in space where the diffusion kernel is modified, the fact that diffusion is affected by the sphere does not stand out in the FCS trace (Figure 7b). The fact that this reduction in contrast is only minor implies that our model supports the common assumption that the modification of the diffusion kernel is not very important in plasmon-enhanced FCS.

Comparison to Simple Gaussian Models. As experimental FCS data are commonly analyzed modeling the focus as a single Gaussian function, we conclude this paper by attempting to cast the obtained rigorous FCS traces in terms of Gaussian-model estimates for hotspot size and volume. One approach for such comparison is to extract zero time-delay contrasts and 50% roll-off times. In a single-Gaussian model, the apparent focus size x can be written in terms of roll-off time and diffusion constant D as $x = \sqrt{4D\tau_{50}}$. Table 1 lists the zero time-delay contrasts and roll-off times for the various cases in the free diffusion kernel approximation, as well as translations into linear dimensions for the volumes derived from these quantities. The antenna-free confocal (with pinhole) case is described reasonably well by the Gaussian model, so we use it

DOI: 10.1021/acs.jpcc.6b02186
J. Phys. Chem. C 2016, 120, 13684−13692

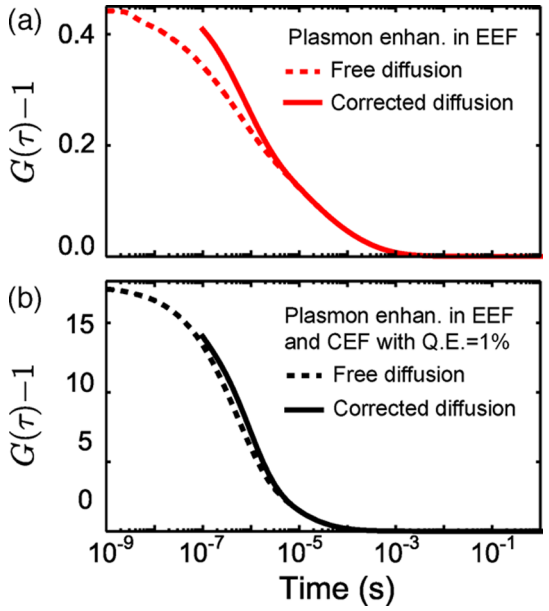

Figure 7. Comparison of FCS traces with the approximate free diffusion kernel (dashed lines) and the exact diffusion kernel (solid lines) accounting for the impenetrable metal sphere. (a) Case of plasmon enhancement only in the EEF. (b) Case of plasmon enhancement in EEF and CEF, in the case of 1% intrinsic fluorophore quantum efficiency. The dashed curves are taken from Figure 5. The exact diffusion result is evaluated only for times beyond 100 ns. At shorter times numerical evaluation would require a finer discretization grid. Note that in each panel the zero-delay time contrast is rigorously identical for both cases.

Table 1. Parameters Extracted from the Zero-Delay Time Contrast and the 50% Roll-Off Time of the Simulated FCS Traces, Assuming Free Diffusion[a]

	zero time-delay contrast			50% roll-off time	
case	contrast	V_{eff}/V_{ref}	$(V_{eff}/\pi^{3/2})^{1/3}$ (nm)	τ_{50} (μs)	$(4D\tau_{50})^{1/2}$ (nm)
confocal	1	1	198	13.4	146
no pinhole	0.102	9.8	425	24	824
EEF	0.44	2.3	261	1	40
QE = 100%	2.37	0.42	149	4.2	82
QE = 1%	17.4	0.0547	77	0.4	25

[a]The contrast translates into an effective volume of the detection function relative to the confocal volume 0.0437 μm^3. As apparent typical length scale, also the widths derived from V_{eff} and from the roll-off time are displayed.

as a reference for the effective volume (first row of Table 1). Taking $s = 2$ and $\sigma = 223/\sqrt{2}$, the effective focal volume according to the correlation contrast is $V_{ref} = \pi^{3/2}\sigma^3 = 0.0437$ μm^3, or 198 nm in linear units. The fact that the roll-off time gives a comparable value for the volume (146 nm) is an indication that the focus is reasonably approximated by a Gaussian distribution.

For the plasmonic cases (last three rows of Table 1), the effective focus derived from contrast and roll-off time differ significantly, especially for the cases dominated by steep field gradients (EEF-only case and QE = 1% case). The fact that the correlation contrast and roll-off time result in very different estimates for the linear dimension of the detection function indicates that the simple Gaussian FCS model is a very poor description. For an experimentalist, this means that using FCS data to estimate plasmonic hot spot size and enhancement on the basis of simple Gaussian FCS intuition is very inaccurate.

Recently, we introduced a two-Gaussian model to quickly estimate FCS contrasts, roll-off times, and full FCS traces for plasmonic hotspots located in a background Gaussian focus.[10] In what follows, we compare FCS traces obtained using the two-Gaussian model to the FCS trace for the QE = 1% case, black line in Figure 5. We fit FCS curves obtained from the two-Gaussian model using as free parameters the hotspot radius and the intensity enhancement. For the Gaussian representing the background focus we have no adjustable parameters, as the background focus is well captured by the parameters listed in Table 1. This situation is akin to experiments in which the background focus could be completely calibrated in a reference measurement.

We use χ^2, the sum of squared deviations between curve and fit, as figure of merit for the goodness of fit. Figure 8a shows the

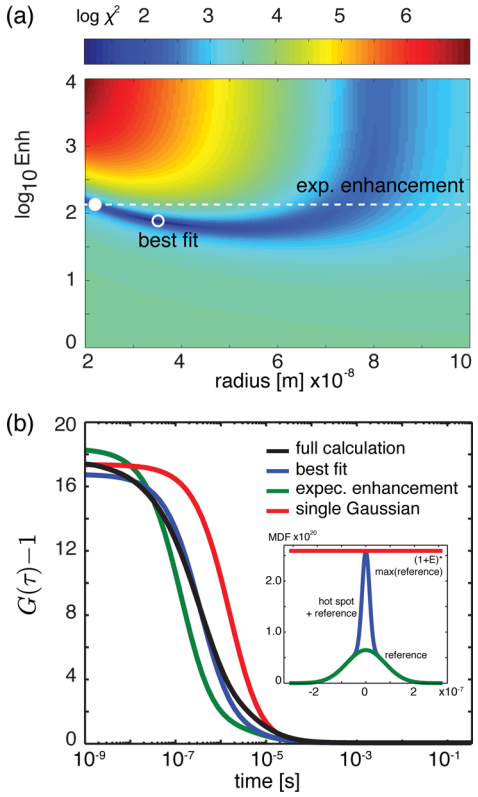

Figure 8. Considering the full calculation for QE = 1% as a reference, we use a two-Gaussian model to fit the FCS curve, using the hotspot radius and the intensity enhancement as free parameters. (a) shows the goodness of the fit parametrized using log χ^2. The empty circle indicates the best fit, the horizontal line indicates the enhancement expected when considering the MDF with and without pinhole, and the full circle shows the best fit for such enhancement. (b) FCS curves for the reference case (black), the best fit (blue), best fit with the expected enhancement (green), and best fit with a single Gaussian (red).

log χ^2 landscape as a function of hotspot radius and intensity enhancement, where we sampled on a time axis that is equidistant on a log scale. Low log χ^2 values, corresponding to the most reasonable fits, expand over a large area of parameters associated with significantly different FCS curves. The minimum log χ^2, marked with an open white circle, corresponds to a radius of 3.5×10^{-8} m and an enhancement

DOI: 10.1021/acs.jpcc.6b02186
J. Phys. Chem. C 2016, 120, 13684−13692

75.8. Evidently, these numbers do not stand in good agreement with actual parameters of the hot spot. For instance, the MDF enhancement for the QE = 1% is about 141, almost twice higher than that corresponding to the best fit. Rather than considering the parameters corresponding to the best fit, one can also ask if putting in known constraints yields a better estimate. For example, one could suppose that the MDF-enhancement of 135 could be measurable, for instance, by analyzing the brightness distribution of time-binned fluorescence bursts.[16] This constraint is indicated by the white dashed line and provides 22 nm as estimate for the hot spot radius (white full circle). Unfortunately, neither this value nor the 35 nm for the best fit is strongly related to an actual length scale that can be pinpointed in the MDF.

For further comparison, Figure 8b shows the FCS curve of the reference QE = 1% case (black) with the FCS curves obtained from the parameters of the best fit (blue) and the best fit for the constrained enhancement (green). The "best fit" (blue curve) reproduces well the 50% roll-off time of the reference case but underestimates the contrast and therefore the volume. The parameters of the best fit constrained to the expected enhancement result in a FCS curve (green) which both overestimates the contrast and underestimates the 50% roll-off time. These curves, based on the two-Gaussian model, are still a better fit than what is obtained with a single-Gaussian model (shown as a red curve and obtained by fixing the contrast). However, Figure 8b shows that even when a two-Gaussian model can give reasonably consistent fits, derived values for contrast and roll-off time can be significantly off.

METHODS

We numerically implemented FCS correlation integrals by tabulating the rigorous solution for the electromagnetic field and for the diffusion kernel. For the diffusion kernel, we created a look-up table of approximately 10^{10} total entries after symmetry reduction. We tabulated values for source and detection points with a spatial resolution of 3 nm over a total range of $r,r' < 1.7\ \mu$m (well in excess of the volume expected to contribute to FCS correlation) at time slices of $K_a(r, r', \tau = t - t')$ equidistant on a logarithmic time axis (starting at 0.1 μs, ending at 1 s, with factors of 1.33 time increment) chosen to match the diffusion behavior expected for rhodamine 6G in water. To tabulate the electromagnetic field distribution, we calculated the plane wave Mie solution (terms up to $n = 45$) on the same (r,θ,ϕ) grid used in the diffusion calculations and performed the back-aperture integral in eq 5 as a discrete sum, sampling the back aperture (up to $\sin\theta = 0.95$ in water, $n = 1.33$, NA = 1.26) with 1800 incident wave vectors.

Using the tabulated diffusion kernel and Mie solution, we evaluated eq 1 by numerical integration in polar coordinates. For each time slice, we integrated over six discretely sampled spatial coordinates, meaning that the integrand is summed over $>10^{12}$ positions. The computational effort required for the integration reduces considerably because the integrand is invariant upon interchange of $\mathbf{r}$ and $\mathbf{r}'$. As benchmark of the routines, we verified that if the diffusion kernel and the focal field are taken as Gaussian, the numerically obtained FCS traces match the textbook expression in eq 2 very well. We find accurate results for all time slices longer than the characteristic diffusion time $\Delta r^2/D$ required to diffuse over the chosen spatial discretization grid size (10 ns at 2 nm discretization).

CONCLUSIONS

We presented a theoretical analysis of plasmon-enhanced FCS for the canonical case of a plasmonic Mie sphere as optical antenna. For this scenario widely disparate FCS contrast enhancements between 2 and 10^4 have been reported. Our main prediction is that FCS contrasts enhancement should be only modest, between 2-fold and 20-fold depending on whether one uses near-unity or near-zero internal quantum efficiency fluorophores. This conclusion holds irrespective of whether one approximates the antenna as permeable or impenetrable for diffusion, as we verified that this approximation only results in a very small correction to the correlation curves.

As regards practical implications, while one could always use plasmon-enhanced FCS substrates for *relative* measurements of concentration and diffusion constants, this will require careful calibration on a fluorophore solution that not only has known concentration and diffusion constant but also the exact same intrinsic quantum efficiency. As soon as *absolute* measurements are attempted, or when attempting determination of plasmon hot spot enhancement and size using FCS traces with a known reference solution, one has to face the fact that since the actual MDF shape is complex, none of its parameters can be reasonably retrieved from simple FCS models. Our experience with the numerical implementation further shows that predicting FCS traces from evaluation of eq 1 is quite a time and resource consuming task because the input quantities, such as particle response to a focused beam and L(R)DOS, need to be sampled with nanometer resolution but yet micrometer range. Hence one needs to evaluate these functions over distinct spatial locations (10^7 in our case), while the integrals ran over typically 10^{15} sampling points (for each time τ).

Furthermore, our theory could equally be used to analyze dielectric FCS experiments using spherical scatters. In particular we note that dielectric microspheres have been proposed as lensing elements, as they generate a diffraction limited focus in their shadow when illuminated by a plane wave.[38,39]

AUTHOR INFORMATION

Corresponding Author

*E-mail: f.koenderink@amolf.nl. Phone: +31 20 7547189.

Notes

The authors declare no competing financial interest.

ACKNOWLEDGMENTS

This work is part of the research program of the Foundation for Fundamental Research on Matter (FOM), which is part of The Netherlands Organization for Scientific Research (NWO). This work is supported by NanoNextNL, a micro- and nanotechnology consortium of the Government of The Netherlands, and 130 partners.

REFERENCES

(1) Magde, D.; Elson, E.; Webb, W. W. Thermodynamic Fluctuations in a Reacting System - Measurement by Fluorescence Correlation Spectroscopy. *Phys. Rev. Lett.* **1972**, *29*, 705−708.

(2) Schwille, P.; Bieschke, J.; Oehlenschläger, F. Kinetic Investigations by Fluorescence Correlation Spectroscopy: the Analytical and Diagnostic Potential of Diffusion Studies. *Biophys. Chem.* **1997**, *66*, 211−228.

(3) Lakowicz, J. R. *Principles of Fluorescence Spectroscopy*, 3rd ed; Springer: New York, 2006.

(4) Mütze, J.; Ohrt, T.; Schwille, P. Fluorescence correlation spectroscopy in vivo. *Laser Photonics Rev.* **2011**, *5*, 52−67.

DOI: 10.1021/acs.jpcc.6b02186
J. Phys. Chem. C 2016, 120, 13684−13692

(5) Levene, M. J.; Korlach, J.; Turner, S. W.; Foquet, M.; Craighead, H. G.; Webb, W. W. Zero-mode waveguides for single-molecule analysis at high concentrations. *Science* **2003**, *299*, 682−686.
(6) Lakowicz, J. R.; Ray, K.; Chowdhury, M.; Szmacinski, H.; Fu, Y.; Zhang, J.; Nowaczyk, K. Plasmon-controlled fluorescence: a new paradigm in fluorescence spectroscopy. *Analyst* **2008**, *133*, 1308−1346.
(7) Estrada, L. C.; Aramendia, P. F.; Martinez, O. E. 10000 times volume reduction for fluorescence correlation spectroscopy using nano-antennas. *Opt. Express* **2008**, *16*, 20597−20602.
(8) Wenger, J.; Rigneault, H. Photonic Methods to Enhance Fluorescence Correlation Spectroscopy and Single Molecule Fluorescence Detection. *Int. J. Mol. Sci.* **2010**, *11*, 206−221.
(9) Choudhury, S. D.; Ray, K.; Lakowicz, J. R. Silver Nanostructures for Fluorescence Correlation Spectroscopy: Reduced Volumes and Increased Signal Intensities. *J. Phys. Chem. Lett.* **2012**, *3*, 2915−2919.
(10) Langguth, L.; Koenderink, A. F. A simple model for plasmon enhanced fluorescence correlation spectroscopy. *Opt. Express* **2014**, *22*, 15397−15409.
(11) Novotny, L.; Hecht, B. *Principles of Nano-Optics*; Cambridge University Press, 2006.
(12) Gerard, D.; Wenger, J.; Bonod, N.; Popov, E.; Rigneault, H.; Mahdavi, F.; Blair, S.; Dintinger, J.; Ebbesen, T. W. Nanoaperture-enhanced fluorescence: Towards higher detection rates with plasmonic metals. *Phys. Rev. B: Condens. Matter Mater. Phys.* **2008**, *77*, 045413.
(13) Giannini, V.; Fernandez-Dominguez, A. I.; Heck, S. C.; Maier, S. A. Plasmonic Nanoantennas: Fundamentals and Their Use in Controlling the Radiative Properties of Nanoemitters. *Chem. Rev.* **2011**, *111*, 3888−3912.
(14) Kinkhabwala, A.; Yu, Z.; Fan, S.; Moerner, W. E. Fluorescence Correlation Spectroscopy at High Concentrations Using Gold Bowtie Nanoantennas. *Chem. Phys.* **2012**, *406*, 3−8.
(15) Punj, D.; Mivelle, M.; Moparthi, S. B.; van Zanten, T. S.; Rigneault, H.; van Hulst, N. F.; Garcia-Parajo, M. F.; Wenger, J. A plasmonic 'antenna-in-box' platform for enhanced single-molecule analysis at micromolar concentrations. *Nat. Nanotechnol.* **2013**, *8*, 512−516.
(16) Yuan, H.; Khatua, S.; Zijlstra, P.; Yorulmaz, M.; Orrit, M. Thousand-fold Enhancement of Single-Molecule Fluorescence Near a Single Gold Nanorod. *Angew. Chem., Int. Ed.* **2013**, *52*, 1217−1221.
(17) Kinkhabwala, A.; Yu, Z.; Fan, S.; Avlasevich, Y.; Müllen, K.; Moerner, W. E. Large Single-Molecule Fluorescence Enhancements Produced by a Bowtie Nanoantenna. *Nat. Photonics* **2009**, *3*, 654−657.
(18) Khatua, S.; Paulo, P. M. R.; Yuan, H.; Gupta, A.; Zijlstra, P.; Orrit, M. Resonant Plasmonic Enhancement of Single-Molecule Fluorescence by Individual Gold Nanorods. *ACS Nano* **2014**, *8*, 4440−4449.
(19) Wang, Q.; et al. Fluorescence correlation spectroscopy near individual gold nanoparticle. *Chem. Phys. Lett.* **2011**, *503*, 256−261.
(20) Punj, D.; de Torres, J.; Rigneault, H.; Wenger, J. Gold nanoparticles for enhanced single molecule fluorescence analysis at micromolar concentration. *Opt. Express* **2013**, *21*, 27338−27343.
(21) Lu, G.; Liu, J.; Zhang, T.; Li, W.; Hou, L.; Luo, C.; Lei, F.; Manfait, M.; Gong, Q. Plasmonic near-field in the vicinity of a single gold nanoparticle investigated with fluorescence correlation spectroscopy. *Nanoscale* **2012**, *4*, 3359−3364.
(22) Mertens, H.; Koenderink, A. F.; Polman, A. Plasmon-Enhanced Luminescence Near Noble-Metal Nanospheres: Comparison Of Exact Theory and an Improved Gersten and Nitzan Model. *Phys. Rev. B: Condens. Matter Mater. Phys.* **2007**, *76*, 115123.
(23) von der Hocht, I.; Enderlein, J. Fluorescence correlation spectroscopy in cells: Confinement and excluded volume effects. *Exp. Mol. Pathol.* **2007**, *82*, 142−146.
(24) Johnson, P. B.; Christy, R. W. Optical Constants of the Noble Metals. *Phys. Rev. B: Condens. Matter Mater. Phys.* **1972**, *6*, 4370−4379.
(25) Mishchenko, M. I.; Travis, L. D.; Lacis, A. A. *Scattering, Absorption, and Emission of Light by Small Particles*; Cambridge University Press: Cambridge, U.K., 2002.
(26) Tai, C. T. *Dyadic Green Functions in Electromagnetic Theory*, 2nd ed.; IEEE Press, 1994.
(27) Novotny, L.; Hecht, B. *Principles of Nano Optics*; Cambridge University Press, 2006.
(28) Hess, S. T.; Huang, S. H.; Heikal, A. A.; Webb, W. W. Biological and chemical applications of fluorescence correlation spectroscopy: A review. *Biochemistry* **2002**, *41*, 697−705.
(29) Enderlein, J.; Gregor, I.; Patra, D.; Dertinger, T.; Kaupp, U. B. Performance of Fluorescence Correlation Spectroscopy for Measuring Diffusion and Concentration. *ChemPhysChem* **2005**, *6*, 2324−2336.
(30) Bharadwaj, P.; Deutsch, B.; Novotny, L. Optical Antennas. *Adv. Opt. Photonics* **2009**, *1*, 438−483.
(31) Taminiau, T. H.; Stefani, F. D.; van Hulst, N. F. Enhanced directional excitation and emission of single emitters by a nano-optical Yagi-Uda antenna. *Opt. Express* **2008**, *16*, 10858−10866.
(32) Agio, M., Alù, A., Eds. *Optical Antennas*; Cambridge University Press, 2013.
(33) El-Dardiry, R. G. S.; Faez, S.; Lagendijk, A. Classification of light sources and their interaction with active and passive environments. *Phys. Rev. A: At., Mol., Opt. Phys.* **2011**, *83*, 031801.
(34) Carslaw, H. S.; Jaeger, J. C. *Conduction of Heat in Solids*; Clarendon Press: Oxford, U.K., 1959.
(35) Samiee, K. T.; Moran-Mirabal, J. M.; Cheung, Y. K.; Craighead, H. G. Zero Mode Waveguides for Single-Molecule Spectroscopy on Lipid Membranes. *Biophys. J.* **2006**, *90*, 3288−3299.
(36) Vobornik, D.; Banks, D. S.; Lu, Z.; Fradin, C.; Taylor, R.; Johnston, L. J. Fluorescence correlation spectroscopy with sub-diffraction-limited resolution using near-field optical probes. *Appl. Phys. Lett.* **2008**, *93*, 163904.
(37) Manzo, C.; van Zanten, T. S.; Garcia-Parajo, M. F. Nanoscale Fluorescence Correlation Spectroscopy on Intact Living Cell Membranes with NSOM Probes. *Biophys. J.* **2011**, *100*, L8−L10.
(38) Gérard, D.; Wenger, J.; Devilez, A.; Gachet, D.; Stout, B.; Bonod, N.; Popov, E.; Rigneault, H. Strong electromagnetic confinement near dielectric microspheres to enhance single-molecule fluorescence. *Opt. Express* **2008**, *16*, 15297−15303.
(39) Devilez, A.; Stout, B.; Bonod, N.; Popov, E. Spectral analysis of three-dimensional photonic jets. *Opt. Express* **2008**, *16*, 14200−14212.

DOI: 10.1021/acs.jpcc.6b02186
J. Phys. Chem. C 2016, 120, 13684−13692